Chemical Science

ROYAL SOCIETY OF CHEMISTRY

EDGE ARTICLE

View Article Online
View Journal | View Issue

Cite this: *Chem. Sci.*, 2021, **12**, 7467

All publication charges for this article have been paid for by the Royal Society of Chemistry

Received 10th March 2021
Accepted 16th April 2021

DOI: 10.1039/d1sc01418h

rsc.li/chemical-science

Anticancer gold(III)-bisphosphine complex alters the mitochondrial electron transport chain to induce *in vivo* tumor inhibition†

Jong Hyun Kim,[a] Samuel Ofori,[a] Sean Parkin,[a] Hemendra Vekaria,[cd] Patrick G. Sullivan[cde] and Samuel G. Awuah *[ab]

Expanding the chemical diversity of metal complexes provides a robust platform to generate functional bioactive reagents. To access an excellent repository of metal-based compounds for probe/drug discovery, we capitalized on the rich chemistry of gold to create organometallic gold(III) compounds by ligand tuning. We obtained novel organogold(III) compounds bearing a 1,2-bis(diphenylphosphino) benzene ligand, providing structural diversity with optimal physiological stability. Biological evaluation of the lead compound **AuPhos-89** demonstrates mitochondrial complex I-mediated alteration of the mitochondrial electron transport chain (ETC) to drive respiration and diminish cellular energy in the form of adenosine triphosphate (ATP). Mechanism-of-action efforts, RNA-Seq, quantitative proteomics, and NCI-60 screening reveal a highly potent anticancer agent that modulates mitochondrial ETC. **AuPhos-89** inhibits the tumor growth of metastatic triple negative breast cancer and represents a new strategy to study the modulation of mitochondrial respiration for the treatment of aggressive cancer and other disease states where mitochondria play a pivotal role in the pathobiology.

Introduction

Platinum drugs, *e.g.* cisplatin, remain the first-line treatment option for many cancer types.[1,2] The induction of drug resistance and toxic side effects from platinum therapy has prompted the generation of new metal-based anticancer agents.[3–6] Metal complexes with different mechanisms of action in the biological context hold great promise. The mode of action of metal complexes is usually by covalent modification of biomolecules,[7–9] non-covalent interaction with target proteins,[10–12] redox activation by biomolecules,[13–15] and photosensitizer action.[16] This has propelled the broad application of metal-based compounds in the treatment of diseases such as microbial infection, rheumatoid arthritis, diabetes, and cancer.[17] Alternative metals used in recent metal-based drug discovery include ruthenium,[18,19] rhenium,[20,21] osmium,[22,23] and gold.[24–27] Additionally, developing metal-based anticancer compounds with a known mechanism of action, well differentiated from cisplatin is essential to overcome cisplatin resistance and improve therapeutic performance.

Gold compounds are resurging as an important class of therapeutics across a broad range of pathophysiology, but major challenges in gold-based bioinorganic chemistry remain, including: (i) the kinetic lability of gold(III) compounds under physiological conditions; (ii) the lack of a rational design of gold-based drugs; (iii) affinity for thiol-rich proteins and enzymes;[28,29] (iv) incomplete understanding of gold reagent localization in living systems; and (v) difficulty in accessing stable high-valent gold(III) compounds. Significant progress in understanding the structure and reactivity of selected gold(III) complexes has provided new impetus for the use of gold compounds.[30–36] Previous and ongoing contributions to surmount challenges associated with physiologically relevant gold compounds as anticancer libraries through innovative chemistries[37–39] continue to expand *via* the development of new scaffolds including gold-porphyrin,[9,40–44] gold-phosphine,[45–51] and cyclometalated gold variations.[52–57] Additionally, our synthetic efforts have led to the generation of [C^N]-cyclometalated gold(III) compounds, which present strong sigma-donation of electrons to stabilize the gold center.[58,59] Furthermore, we expanded the repertoire of gold-based agents with the synthesis of distorted gold constructs bearing chiral phosphine ligands.[60]

[a]*Department of Chemistry, University of Kentucky, Lexington, KY 40506, USA. E-mail: awuah@uky.edu*

[b]*Center for Pharmaceutical Research and Innovation, College of Pharmacy and Department of Pharmaceutical Sciences, College of Pharmacy, University of Kentucky, Lexington, Kentucky 40536, USA*

[c]*Spinal Cord and Brain Injury Research Center, University of Kentucky, USA*

[d]*Department of Neuroscience, University of Kentucky, USA*

[e]*Lexington Veterans' Affairs Healthcare System, USA*

† Electronic supplementary information (ESI) available: All synthetic procedures, chemical experiments, biological experiments and characterization data. CCDC 2034162 (**AuPhos-81**), 2034159 (**AuPhos-82**), 2034161 (**AuPhos-83**), 2034160 (**AuPhos-84**). For ESI and crystallographic data in CIF or other electronic format see DOI: 10.1039/d1sc01418h

Accumulating evidence shows that aggressive tumors including triple negative breast cancer (TNBC, the model system for this report)[61–65] have strong dependence on both glycolytic and oxidative pathways. Thus, a key promising strategy is targeting mitochondrial metabolism for cancer therapy.[66] Rosner *et al.* showed that combining BACH1 targeting with oxidative phosphorylation electron transport chain (OXPHOS) inhibition by metformin is an effective TNBC therapy.[67] The lack of potency of metformin has prompted several groups to develop superior inhibitors of OXPHOS as therapeutic agents for several diseases including cancer.[68–73] Parada *et al.* demonstrated the use of a small-molecule, Gboxin, as an inhibitor of OXPHOS to target glioblastoma.[74] Their work revealed that aggressive tumors rely on mitochondrial respiration for their energy needs, which can be exploited for therapeutic gains.

Here, we have synthesized and characterized new organogold(III) compounds supported by a diphenylphosphine benzene ligand. These compounds are stable toward biological thiols and demonstrate enhanced mitochondrial oxygen consumption rate and inducing proton leak in TNBC. Strikingly, in a comparative screening of a reference set of 60 cancer cell lines compiled by the National Cancer Institute (NCI-60) these compounds induce lethality across all tumor types. Whole-cell transcriptomics reveal a broader mechanism of action in addition to the dominant oxidative phosphorylation target supported by quantitative proteomic studies in response to the gold compound, **AuPhos-89**. We tested the efficacy of the lead compound, **AuPhos-89** in a metastatic 4T1 TNBC mouse model and found significant tumor inhibition. Together, these studies demonstrate the translational potential of gold(III) compounds in anticancer drug development.

Results and discussion

Anticancer compound design, synthesis, and characterization

The organogold(III) bearing bisphosphine ligands, herein referred to as the AuPhos class of compounds, were synthesized as part of our research efforts to generate diverse gold compounds for biological evaluation. We rationalized that stabilizing the gold(III) center by efficient ligand tuning will influence biological reactivity and function. To minimize premature deactivation and degradation of anticancer agents, *in vivo*, it is imperative to enhance their kinetic stability. The use of strongly donating phosphorus containing ligands coupled with (C^N)-cyclometalation provides a unique balance between compound stability and efficacy. Optimizing ligands around the gold center decorated with (C^N)-cyclometalation has been hampered by the rapid reductive elimination induced by donor ligands to form C(sp^2)–X bonds. To resolve this, we utilized bisphosphine coupled with mild reaction conditions which minimizes reductive elimination but gives rise to the target compound. We selected diphenylphosphine benzene as the donor ligand of choice and reacted it with a series of cyclometalated gold(III) starting materials for structure activity relationship (SAR) studies. Briefly, treatment of $HAuCl_4$ with the respective benzyl/benzoyl pyridine ligands in refluxing water affords the cyclometalated compounds. Ligand substitution reactions with bisphosphine ligands in chloroform at room temperature overnight resulted in organometallic gold(III) bisphosphine compounds, AuPhos (Fig. 1). It is worth noting that the products of the reaction scheme in Fig. 1A were verified by structural insights obtained by X-ray crystallography data (*vide infra*). Thus, the Au(III)-bisphosphine studied in this work likely existed as organgold(III)-bisphosphine compounds without Au–N (sp^2) coordination or with Au–N (sp^2) coordination as in **AuPhos-83**. Complexes **AuPhos-81**–**AuPhos-89** were characterized by ^{1}H NMR, ^{31}P NMR, ^{13}C NMR spectroscopy (Fig. S1–S24†), and high-resolution mass spectrometry (Fig. S25–S32†). The purity of the compounds was confirmed by elemental analysis. The ^{31}P NMR spectra of these compounds show two characteristic peaks in the downfield region of >50 ppm. The resonances show a doublet, which is as a result of *cis*-P–P coupling. The spectroscopic data obtained were validated by HRMS (ESI) for all compounds, showing a characteristic $[M–Cl]^+$ molecular ion peak. The ionization pattern and isotopic distribution confirm the potential coordination of one chloride ligand to the gold center.

The AuPhos complexes display moisture and air stability. To study the biological stability of AuPhos complexes, reactivity with glutathione (L-GSH), a representative intracellular antioxidant, was evaluated using HPLC in aqueous solution (Fig. S33†). Interestingly, the chromatogram of **AuPhos-89** in the reaction showed little change over the estimated 24 h period. Similarly, stability studies of **AuPhos-89** using ^{1}H-NMR spectroscopy were performed (Fig. S34†). The proton resonances corresponding to **AuPhos-89** or L-GSH in the mixed reaction solution of **AuPhos-89** and L-GSH in DMSO-d_6 were minimally altered after 24 h. Changes in proton resonances at 0 and 1 h seem to be due to the slow solubility of L-GSH in DMSO solvent. Together, these experiments confirm the stability of **AuPhos-89** in the biological environment.

Single crystals of **AuPhos-81**, **82**, and **84** were grown by vapor diffusion of ether into a solution of concentrated gold complex in DMF at 4 °C or room temperature, and **AuPhos-83** was crystallized using acetone/THF. The single crystals were analyzed by X-ray diffraction to determine the molecular structures. The crystal structures solved for **AuPhos-81**, **82** and **84** reveal a four-coordinate structure with the carbon from the arylpyridine bonded to the gold atom, chloride and diphosphine coordinated to the gold atom in a square-planar geometry. Based on the crystal structure of **AuPhos-83**, a cyclometalated compound is obtained, where the arylpyridine ring is bonded through the carbon and nitrogen atoms to the gold. The Au–N bond length is 2.096(4), indicative of a strong bond. The organogold character is defined by the existence of the Au–C bond with a bond length within the range of 2.072(8)–2.0819(19) for **AuPhos-81**, **82** and **84**. In contrast, the Au–C bond for **AuPhos-83** is slightly longer at 2.100(5). Another interesting feature of the crystal structure of **AuPhos-83** is the potential axial interaction of the cationic Au center and chloride ligand. Whereas the observation is found in the solid state with a relatively longer bond length of 2.8790(11), it presents opportunities to investigate the type of interaction or bonding in solution and whether Au(III) systems can

accommodate a fifth coordination. The use of the 1,2-bis(diphenylphosphino)benzene (DPPB) ligand provides a rigid backbone for gold chelation. Table 1 shows selected interatomic bond distances and angles of the crystal structure of **AuPhos-81**, **82**, **83**, and **84** as displayed in Fig. 1. Further analysis of the P1–Au1–Cl1 angles of **AuPhos-81**, **82**, and **84** shows a close to linear angle of ~173–178°. Overall, the structures of organogold(III)-bisphosphine complexes have been elucidated.

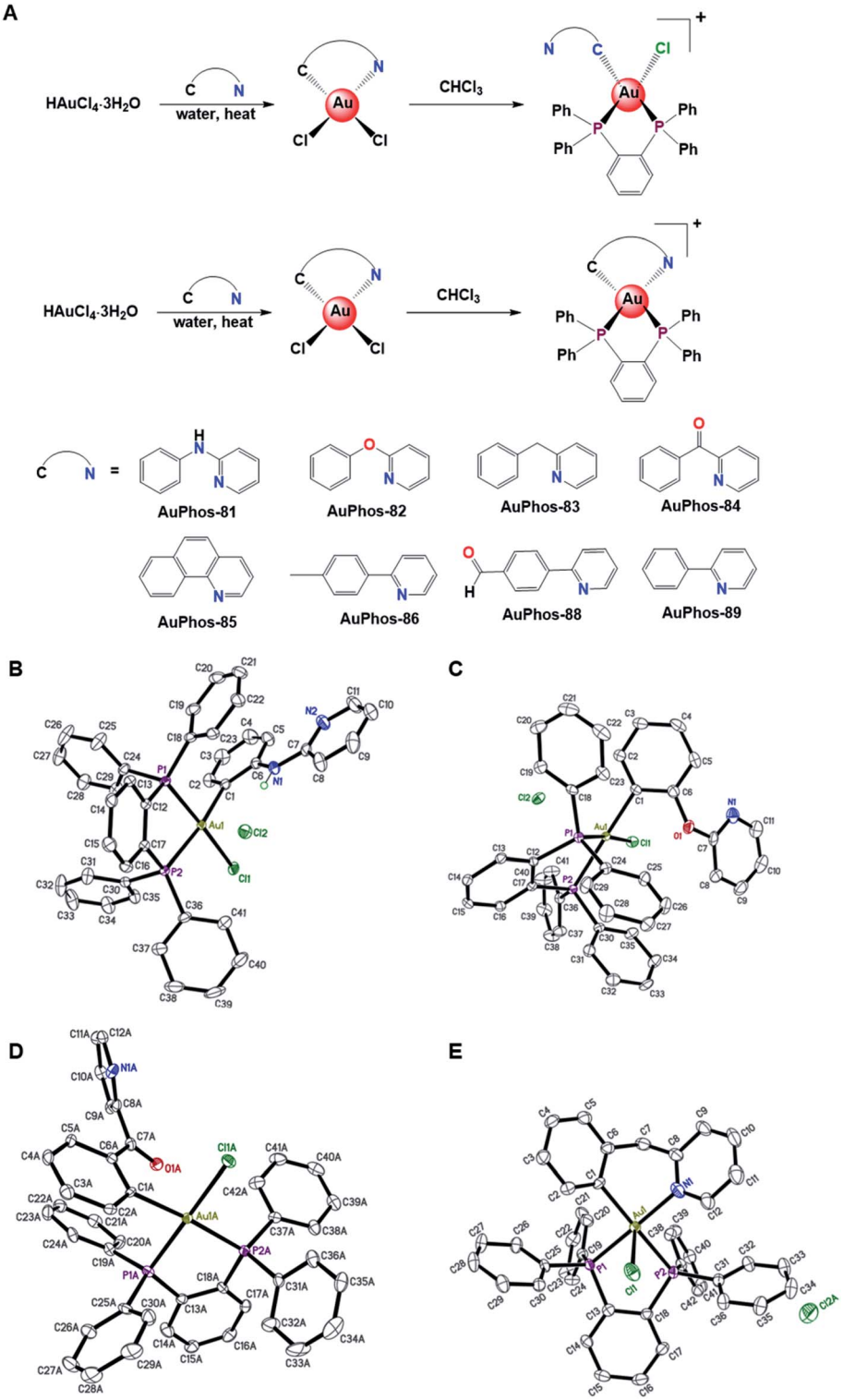

Fig. 1 Chemical structures of AuPhos compounds. (A) Synthetic scheme to access organogold(III) compounds investigated in this study. (B)–(E) Crystal structures of **AuPhos-81**, **82**, **84**, and **83**. Outer-sphere solvent molecules are omitted for clarity. Thermal ellipsoids are shown at the 50% probability level. In (D), only one representative molecule from the asymmetric unit is shown.

Table 1 Selected interatomic distances (Å) and angles (°) from the crystal structures shown in Fig. 1 below

	Gold complexes				
Bond/angle	**AuPhos-81**	**AuPhos-82**	**AuPhos-83**	**AuPhos-84**	
Au1–N1	—	—	2.096(4)	—	—
Au1–C1	2.0819(19)	2.074(3)	2.100(5)	2.079(8)	2.072(8)
Au1–P1	2.2808(5)	2.2843(7)	2.3396(12)	2.289(2)	2.283(2)
Au1–P2	2.3602(5)	2.3451(7)	2.3406(12)	2.341(2)	2.344(2)
Au1–Cl1	2.3387(5)	2.3354(6)	2.8790(11)	2.342(2)	2.341(2)
P1–C24/C25	1.808(2)	1.811(3)	1.797(4)	1.807(8)	1.804(8)
P1–C12/C13	1.8180(19)	1.815(3)	1.810(5)	1.806(9)	1.814(9)
P2–C36/C37	1.808(2)	1.799(3)	1.801(5)	1.800(8)	1.808(8)
C1–Au1–P1	91.10(6)	93.46(7)	96.22(14)	88.7(2)	178.63(7)
N1–Au1–P2	—	—	96.46(13)	—	—
C1–Au1–P2	172.04(6)	175.92(7)	175.16(15)	175.3(2)	175.5(2)
P1–Au1–P2	84.459(17)	82.91(2)	82.76(4)	86.55(8)	86.57(8)
N1–Au1–Cl1	—	—	96.05(14)	—	—
C1–Au1–Cl1	89.76(6)	90.44(7)	97.65(14)	90.5(2)	90.5(2)
P1–Au1–Cl1	176.814(18)	173.47(2)	88.58(4)	178.91(8)	178.63(7)
P2–Au1–Cl1	94.331(17)	93.01(2)	87.07(4)	94.15(8)	93.79(8)

NCI-60 screening

Encouraged by the anti-proliferative potency of the compounds (Table S1 and Fig. S35–S39†), we sought to expand the cell lines used and possibly gain insight into the mechanism of action (MOA). Comparative profiling and recent advances in omics technology have expanded the toolkit for target identification and mechanism of action of bioactive molecules. A phenotypic comparison of compounds with known mechanisms can reveal the MOA of compounds with unknown mechanisms, particularly, metal-based compounds. The use of comparative profiling approaches relies on correlating phenotypes obtained with an unknown compound to those within a set of reference compounds with known MOA. It is inferred that compounds with similar MOA will exhibit similar phenotypes. In 1990, the National Cancer Institute compiled a reference set of 60 cancer cell lines (NCI-60) and profiled the sensitivity of each cell line to a large panel of compounds.[75,76] This has yielded large-scale datasets that are rich resources for the MOA of unknown compounds and target identification. We were interested in assessing the comparative profiles of three of our AuPhos compounds (**AuPhos-83**, **84**, and **89**) in the NCI-60 screening service. Following a single dose screening at 10 μM, the Developmental Therapeutic Program prioritized the compounds for 5-point dose response assays in the NCI-60 panel. The results reveal that **AuPhos-83**, **84** and **89** display profound lethality across all cancer types including breast cancer with GI_{50} in the range of 150 nM–700 nM. All three compounds (**AuPhos-83**, **84**, and **89**) showed excellent results across the NCI-60 panel with unbiased lethal effects, especially in central nervous system (CNS) cancer, melanoma, and renal cancers. Surprisingly, the lethal effect on liquid tumors such as leukemia was relatively diminished compared to the solid tumors in the NCI-60 panel. Thus, we prioritized the compound with superior cell growth inhibitory ability across all cell lines (*i.e.* **AuPhos-89**) for further biological experiments. These results are shown in the ESI (Fig. S40–S42†) and summarized in Fig. 2.

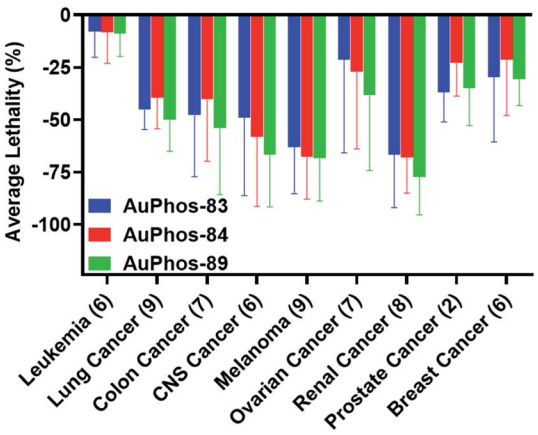

Fig. 2 Summary of the NCI-60 human tumor cell line screen. **AuPhos 83**, **84**, and **89** show superior activity across the panel of cell lines tested including breast. Numbers in parentheses represent the number of cell lines tested for each indication. The breast panel includes TNBC (MDA-MB-231, BT549, Hs578T, MDA-468) and luminal cell lines (MCF7, T47D).

Additionally, the COMPARE algorithm, which is a pattern recognition algorithm, can be used to suggest a putative mechanism or the uniquely distinct mechanism of a given agent. Pearson (PCC) and Spearman correlations (SC) are used to estimate the degree of similarity of a test compound, in this case AuPhos, to compounds with known mechanisms in the NCI-60 database. We used an FDA-approved and investigational compound library from the Cancer Chemotherapy National Service Center (NSC) for comparison. The rationale for this compound set was the well-characterized MOA of approved drugs. We found that the AuPhos compounds screened in the NCI-60 panel had no reliable correlation with the drug set used. The filtering conditions utilized GI50, LC50, and TGI derived from the NCI-60 results obtained for AuPhos. Taken together,

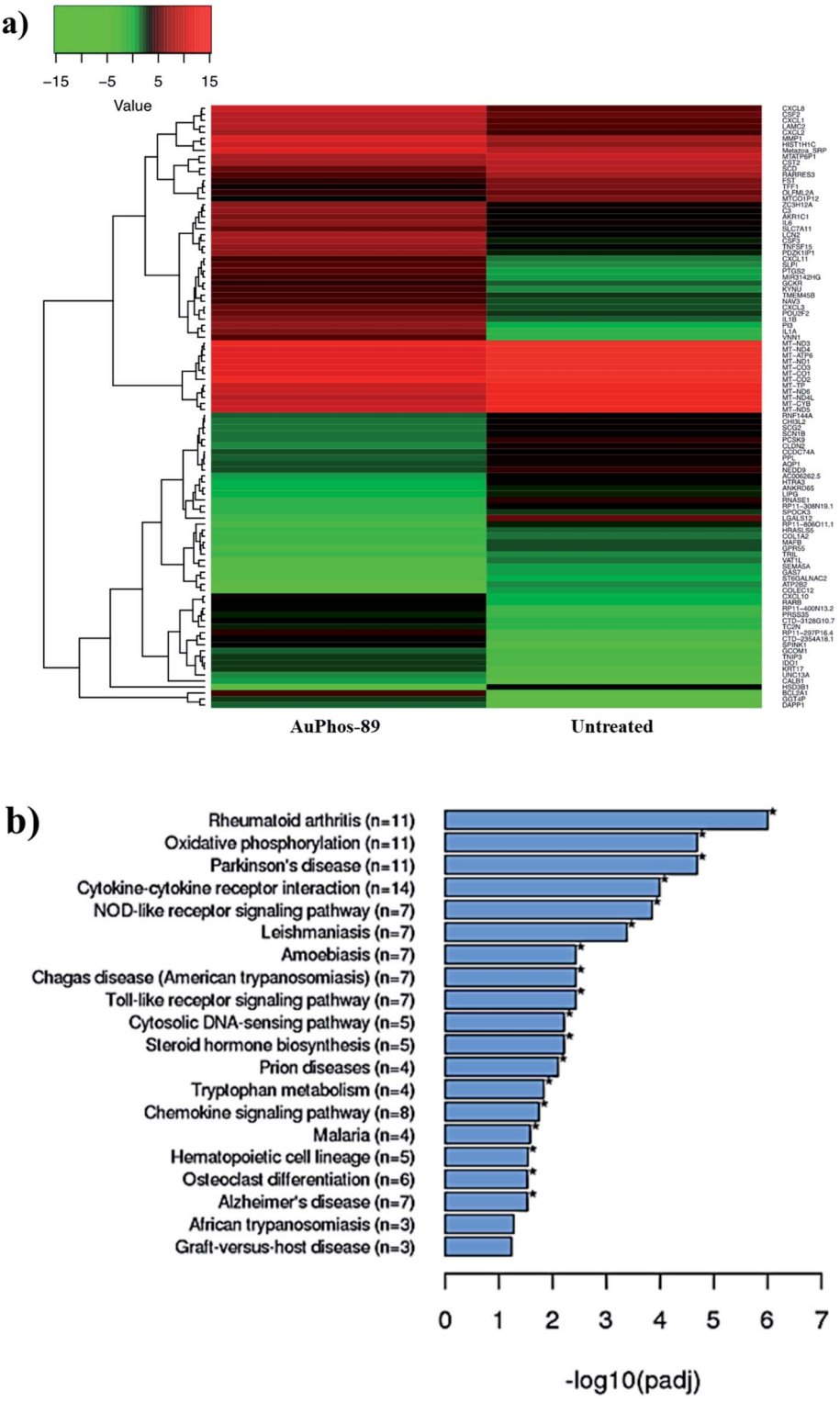

Fig. 3 Whole-cell transcriptomics. (a) Representative heat map of DEGs in response to **AuPhos-89**. (b) KEGG analysis plots outlining varying pathways perturbed upon treatment with **AuPhos-89**. MDA-MB-231 cells were treated with **AuPhos-89** (1 μM for 12 h) and pure RNA isolated for sequencing. Data are representative of two independent replicates.

the comparative profiling of the novel class of gold compounds revealed a different mechanism of action from known drugs, which presents new opportunities for efficacious drugs.

Differential gene expression and biological pathway analysis

Based on the exceptional potency of the AuPhos class of compounds and different mechanism of action as derived from the NCI-60 screening, we employed a systems biology approach

to assist in our quest to unravel the mechanism of action or validate findings from comparative profiling. We used RNA sequencing to determine differential gene expression in MDA-MB-231 cells in response to treatment with 1 μM of **AuPhos-89** for 12 h. Briefly, MDA-MB-231 cells were exposed to **AuPhos-89** and following the isolation of highly pure RNA, RNA-sequencing was performed for both control- and AuPhos-treated cells with ~30 million 50-bp paired-end reads generated per sample using the Illumina Hi-seq. Sequence reads were mapped to the hg19 (GRCh37) human genome. We found 922 DEG with 83 upregulated and 94 downregulated genes in response to AuPhos (Fig. 3a). Kyoto encyclopaedia of genes and genomes (KEGG)[77–79] (Fig. 3b) pathway analysis uncovered potential processes perturbed by **AuPhos-89**. The pathway analysis software employed is an extensive library database capable of integrating chemical and biological pathway perturbation processes and is well suited for drug development studies. Differentially expressed genes that contributed to the top five pathways in response to **AuPhos-89** included rheumatoid arthritis, oxidative phosphorylation, Parkinson's disease, cytokine–cytokine receptor interaction, and NOD-like receptor signaling. Interestingly, these processes are related to inflammation, which is chiefly regulated by the mitochondria and linked to metabolism. Several differentially expressed genes were related to the electron transport chain, the driver of oxidative phosphorylation. Thus, we hypothesized that **AuPhos-89** induces cell death by modulating oxidative phosphorylation and redox pathways in breast cancer cells. Recent findings suggest OXPHOS as a viable therapeutic target in cancer including breast cancer. This led us to investigate the effect of **AuPhos-89** on mitochondrial metabolism.

Cellular and mitochondrial uptake of AuPhos

In our efforts to deepen the insight into the mechanism of action of AuPhos, we sought to examine the intracellular accumulation. Cell permeability is an essential physicochemical property of drug-like molecules or chemical probes. The ability of compounds to cross the cell membrane to induce cytotoxic effects or engage their targets contributes to their efficacy. To study the intracellular uptake for AuPhos, we performed whole-cell uptake experiments in OVCAR8 cells using **AuPhos-83**, **84** and **89** and found that an appreciable amount of compound was detected in cells after 15 h (Fig. S43†). Compound uptake was confirmed by measuring gold accumulation using graphite furnace atomic absorption spectroscopy (GF-AAS). Given that the preliminary targets identified *via* NCI-60 screening and RNA-seq were localized in the mitochondria, quantification of AuPhos in mitochondria is imperative. We further assessed compound uptake in mitochondria organelle fractions of MDA-MB-231 cells after incubation with **AuPhos-89** (Fig. 4). This was to confirm mitochondria localization given the dominant oxidative phosphorylation pathway identified. The gold content measured by GF-AAS showed that the gold compound taken up in the mitochondria of cancer cells is significantly higher (>5-fold) than normal cell mitochondria (Fig. 4B and C). This could be attributed to the high mitochondrial membrane potential in cancer cells compared to normal cells. Additionally, gold uptake by the mitochondria of MDA-MB-231 compared to NCM460 demonstrates the selective accumulation of the compound for cancerous cells in comparison to normal cells. The high degree of cancer cell selectivity is driven by the upregulation of vitamin and fatty acid transporters in cancer cells. In addition, the lipophilic cationic character of AuPhos facilitates mitochondrial uptake. Together, these findings suggest that **AuPhos-89** is taken up into intracellular locations of cancer cells, specifically into the mitochondria.

Role of AuPhos in enhancing mitochondrial respiration

The direct interaction and effect of **AuPhos-89** on mitochondria was investigated to assess mitochondrial bioenergetics. A characteristic hallmark of mitochondrial uncoupling activity is the increase of mitochondrial oxygen consumption rate (OCR), even in the presence of F_oF1 ATP synthase inhibitors including oligomycin. Using isolated mitochondria from the liver of C57BL/6J mice, **AuPhos-89** at a concentration of 1 μM increased oxygen consumption in the presence of oligomycin (Fig. 5A) as determined using a Seahorse XF analyzer. This phenomenon was dose-dependent up to about 10 μM. Moreover, the induction of OCR was independent of Ca^{2+} (Fig. 5B). Furthermore, at the same concentrations, **AuPhos-89** acutely induced proton

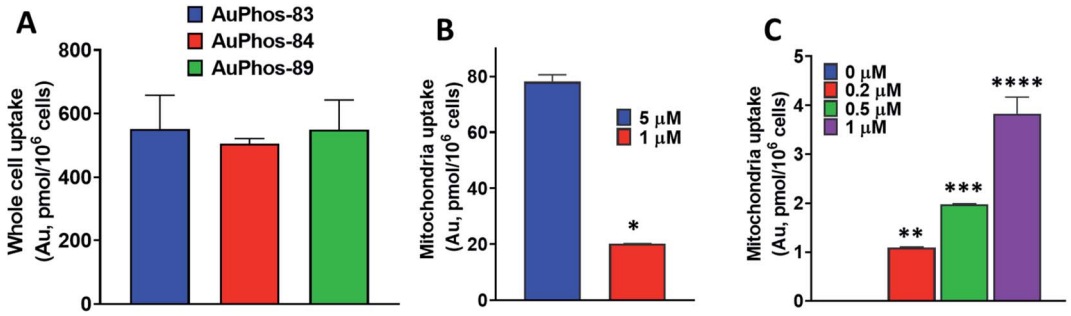

Fig. 4 Cellular and mitochondrial uptake study. (A) Whole-cell uptake results of representative AuPhos compounds in MDA-MB-231 cells. (B) Mitochondrial accumulation of **AuPhos-89** in breast cancer epithelial cells. (C) Mitochondrial accumulation of **AuPhos-89** in normal colon epithelial cells (NCM 460). Data are a mean of three independent replicates. For (B), unpaired *t*-test, $*P < 0.0001$, for (C), ordinary one-way ANOVA, $**P < 0.01$, $***P < 0.001$, $****P < 0.0001$.

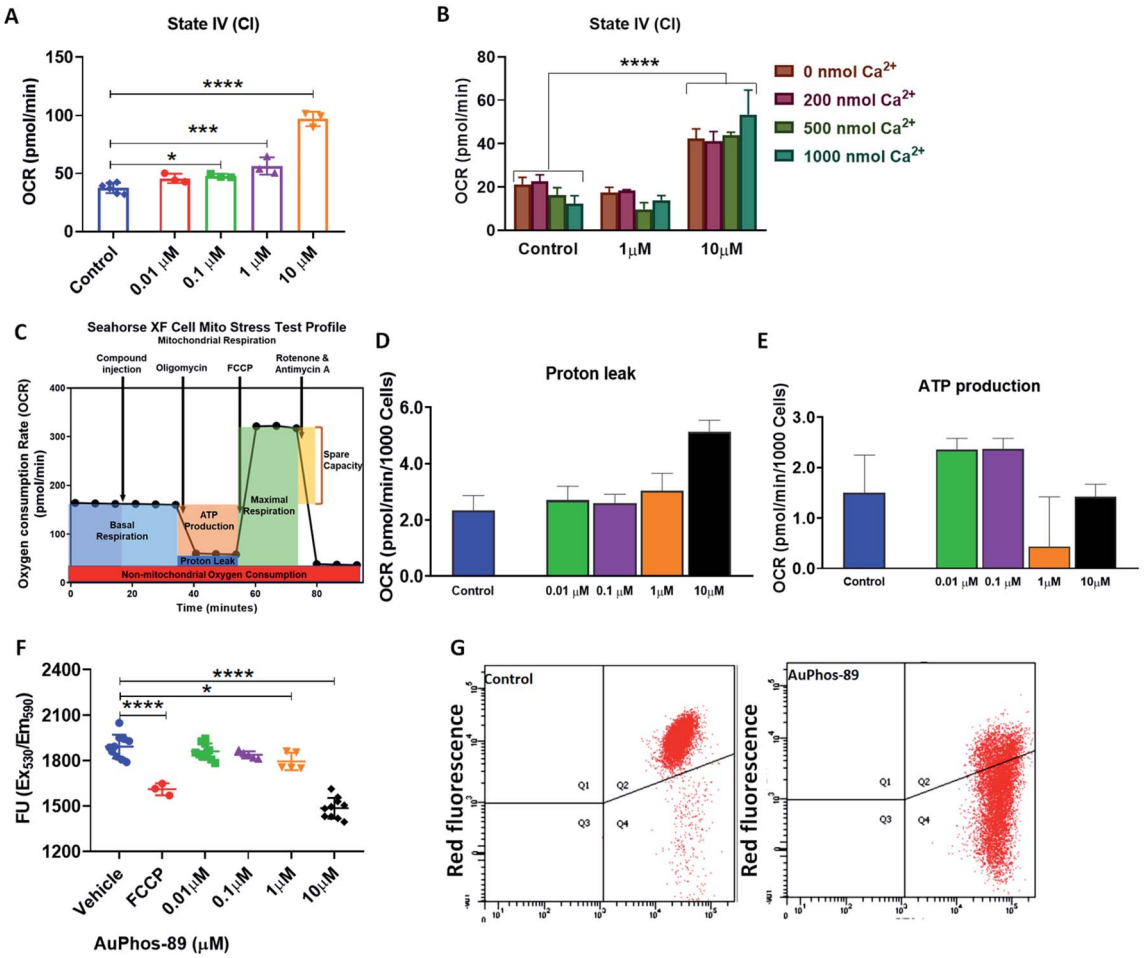

Fig. 5 Effect of AuPhos on bioenergetics. (A) OCR mediated by complex I (State IV) from the effect of **AuPhos-89** on isolated liver mitochondria in the presence of oligomycin. (B) OCR mediated by complex I (State IV) from the effect of **AuPhos-89** on isolated liver mitochondria in the presence of oligomycin and Ca^{2+}. (C) Schematic diagram of the mitochondrial respiration experiment. (D) Proton leak extrapolated from the mito-stress test of MDA-MB-231 cells treated with **AuPhos-89**, (E) ATP production extrapolated from the mito-stress test of **AuPhos-89** treated MDA-MB-231 cells. (F) Changes in the membrane potential of MDA-MB-231 cells depending on the concentration of **AuPhos-89** using TMRE assay and FCCP as control. (G) Mitochondrial membrane potential measured by FACS of MDA-MB-231 cells, control (left), **AuPhos-89**-treated (middle) using JC-1 assay. Ordinary one-way or two-way ANOVA, $*P < 0.01$ and $****P < 0.0001$.

leak in live MDA-MB-231 cells (Fig. 5D) with diminished ATP production (Fig. 5E). Assessment of the mitochondrial membrane potential (MMP) indicated that there was depolarization of the MMP of MDA-MB-231 cells using the TMRE (Fig. 5F) or JC-1 assay at short compound exposure periods (Fig. 5G). Our results support the mitochondrial OXPHOS as a potential target of **AuPhos-89**.

Cellular responses evoked by AuPhos

Analysis of cell population in the different phases of the cell cycle revealed no significant changes to the cell cycle, indicating that the compound does not stall cells in these phases under the treatment condition used (Fig. 6A). The DNA binding agent, cisplatin, is known to induce S and G2/M cell cycle arrest in a number of cell lines, supporting its mechanism of DNA cross-linking. When MDA-MB-231 cells were exposed to **AuPhos-89** at 1 μM for 15 h, a significant population (~40%) of cells were in early to late apoptosis as detected by FACS (Fig. S43A†). As expected, the control treated with hydrogen peroxide showed significant apoptosis (Fig. S44B†). The results suggest that AuPhos induces significant apoptosis as a mode of cell death in breast cancer cells. Furthermore, to determine if **AuPhos-89** induces apoptosis through the caspase-mediated apoptotic pathway, we performed western blotting to assess the induction of caspases and cleaved PARP (Fig. S44C†). We found that **AuPhos-89** activates cleaved caspases, PARP and the cellular energy regulator, AMPK (Fig. 6B), a hallmark of apoptosis. We investigated global changes in proteins using quantitative proteomics after 12 h of exposing MDA-MB-231 cells to **AuPhos-89** at 1 μM. In this tandem mass tag (TMT)-based quantification, protein was extracted from cryo-preserved cell pellets and following tryptic digestion, TMT-labeling was performed. After fractionation, tandem LC-MS/MS was conducted and database search against HUMAN protein database was carried out. Proteins of relative quantification were divided into two categories. A quantitative ratio over 1.5 was considered upregulation while a quantitative ratio less than 1/1.5 was considered as

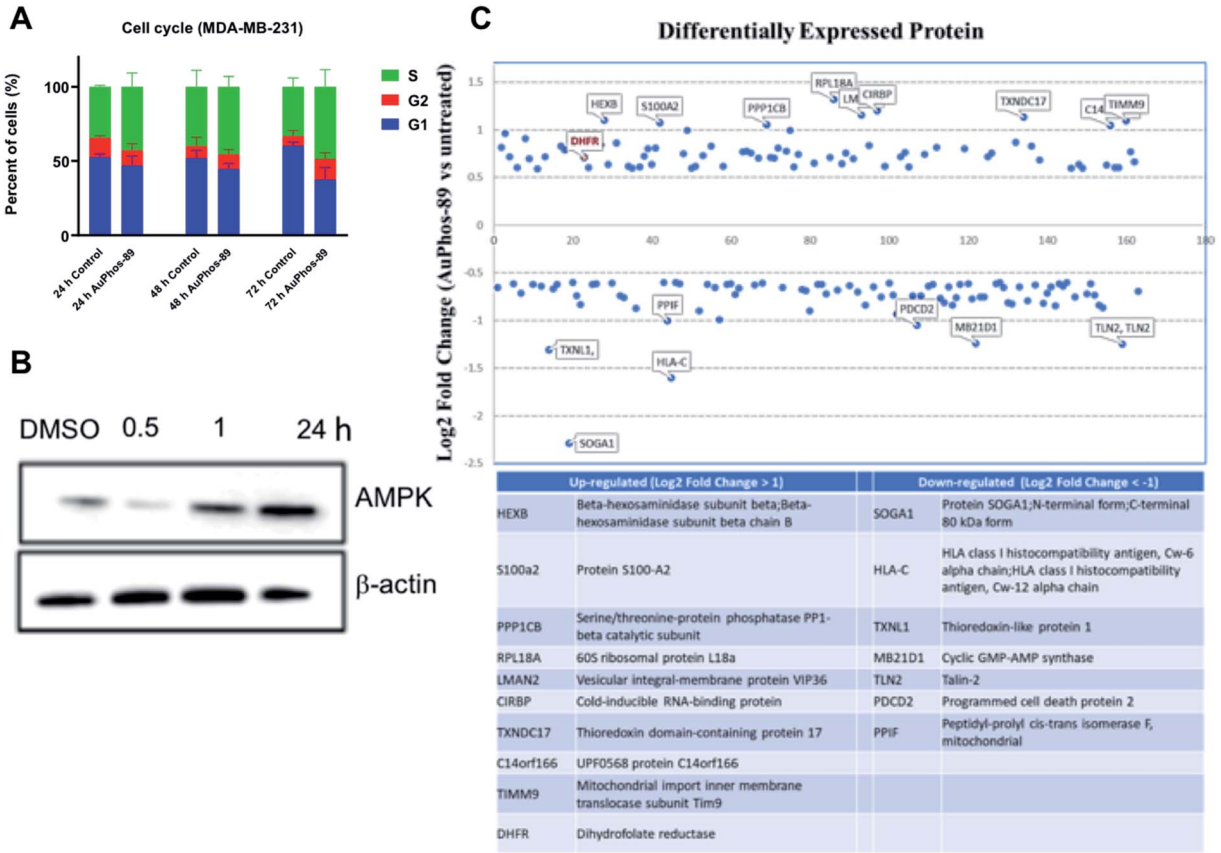

Up-regulated (Log2 Fold Change > 1)		Down-regulated (Log2 Fold Change < -1)	
HEXB	Beta-hexosaminidase subunit beta;Beta-hexosaminidase subunit beta chain B	SOGA1	Protein SOGA1;N-terminal form;C-terminal 80 kDa form
S100a2	Protein S100-A2	HLA-C	HLA class I histocompatibility antigen, Cw-6 alpha chain;HLA class I histocompatibility antigen, Cw-12 alpha chain
PPP1CB	Serine/threonine-protein phosphatase PP1-beta catalytic subunit	TXNL1	Thioredoxin-like protein 1
RPL18A	60S ribosomal protein L18a	MB21D1	Cyclic GMP-AMP synthase
LMAN2	Vesicular integral-membrane protein VIP36	TLN2	Talin-2
CIRBP	Cold-inducible RNA-binding protein	PDCD2	Programmed cell death protein 2
TXNDC17	Thioredoxin domain-containing protein 17	PPIF	Peptidyl-prolyl cis-trans isomerase F, mitochondrial
C14orf166	UPF0568 protein C14orf166		
TIMM9	Mitochondrial import inner membrane translocase subunit Tim9		
DHFR	Dihydrofolate reductase		

Fig. 6 Cellular responses to **AuPhos-89**. (A) Cell cycle distribution by PI staining: br graph representing the percentage of cells in G1, G2, and S. MDA-MB-231 cell bars represent an average of 3 measurements. Error bars represent means ± SD. (B) Time-dependent activation of AMPKα and of MDA-MB-231 treated with **AuPhos-89** (1 μM) and analyzed by immunoblotting. (C) TMT-labelled quantitative proteomics. Differentially expressed protein data; only Log_2 FC values more than 1 and less than −1 were extracted and displayed. Proteins with high values are shown in the table. MDA-MB-231 cells were treated with **AuPhos-89** (1 μM, 12 h).

downregulation. We found a total of 163 differentially expressed proteins, 75 of which were upregulated and 88 downregulated (Fig. 6C, ESI table†). Additionally, protein-related mitochondrial metabolism including ADP-ribosylation 4, glutathione-S-transferase, thioredoxin, and enzymes in the glucose pathway was upregulated to compensate for energy deprivation by mitochondrial stress. Overall, the proteomics study supports the other profiling studies described in this work and clearly lays out a systematic pipeline to study new metal-based agents and elucidate their mode of action in an unbiased way.

In vivo anticancer potential of AuPhos-89

Despite the augmented *in vitro* potency and the novel mechanistic activities reported with other experimental metal-based anticancer agents, many of these compounds have been limited by lack of preclinical evaluation in animal models.

We evaluated the relative *in vivo* antitumor efficacy of **AuPhos-89** as compared to vehicle control. A murine 4T1 cell-line syngeneic of the TNBC model was employed, and **AuPhos-89** was administered by 3 weekly IV injections at a dose equivalent of 10 mg kg^{-1} ($n = 5$ mice per treatment group). A separate group of mice was administered equal volumes of vehicle control at the same time points and *via* the analogous route. During the first three days after tumor cell implantation and prior to treatment, all mice exhibited equivalent rates of tumor growth. After the first injection, the growth rate of the **AuPhos-89** treated group decreased significantly, and this trend was maintained until the end of the experiment (Fig. 7A).

We conducted a separate experiment to compare the antitumor efficacy of the gold compound, **AuPhos-89**, with that of the FDA approved platinum drug, cisplatin, which is used to treat TNBC. **AuPhos-89** (10 mg kg^{-1}) was injected by the intraperitoneal route, and cisplatin was administered at a low concentration of 3 mg kg^{-1} *via* intraperitoneal injection due to the toxicity of the drug. Compared with the control group, significant tumor inhibition was observed in the two treatment groups. The weight was kept constant in all the control groups and the experimental group (Fig. 7).

Tissue biodistribution of therapeutic agents can shed light on drug accumulation and clearance in various organs within test animals. Biodistribution contributes to validating a drug candidate for clinical use. To determine the *in vivo* biodistribution profile and to validate the effective delivery of the gold compound, we injected **AuPhos-89** intravenously at 10 mg kg^{-1} into female BALB/c mice. After respective time points of 1 h and 24 h, mice were euthanized. Organs including heart, lung, liver, spleen, kidney, and tumor were excised and the gold

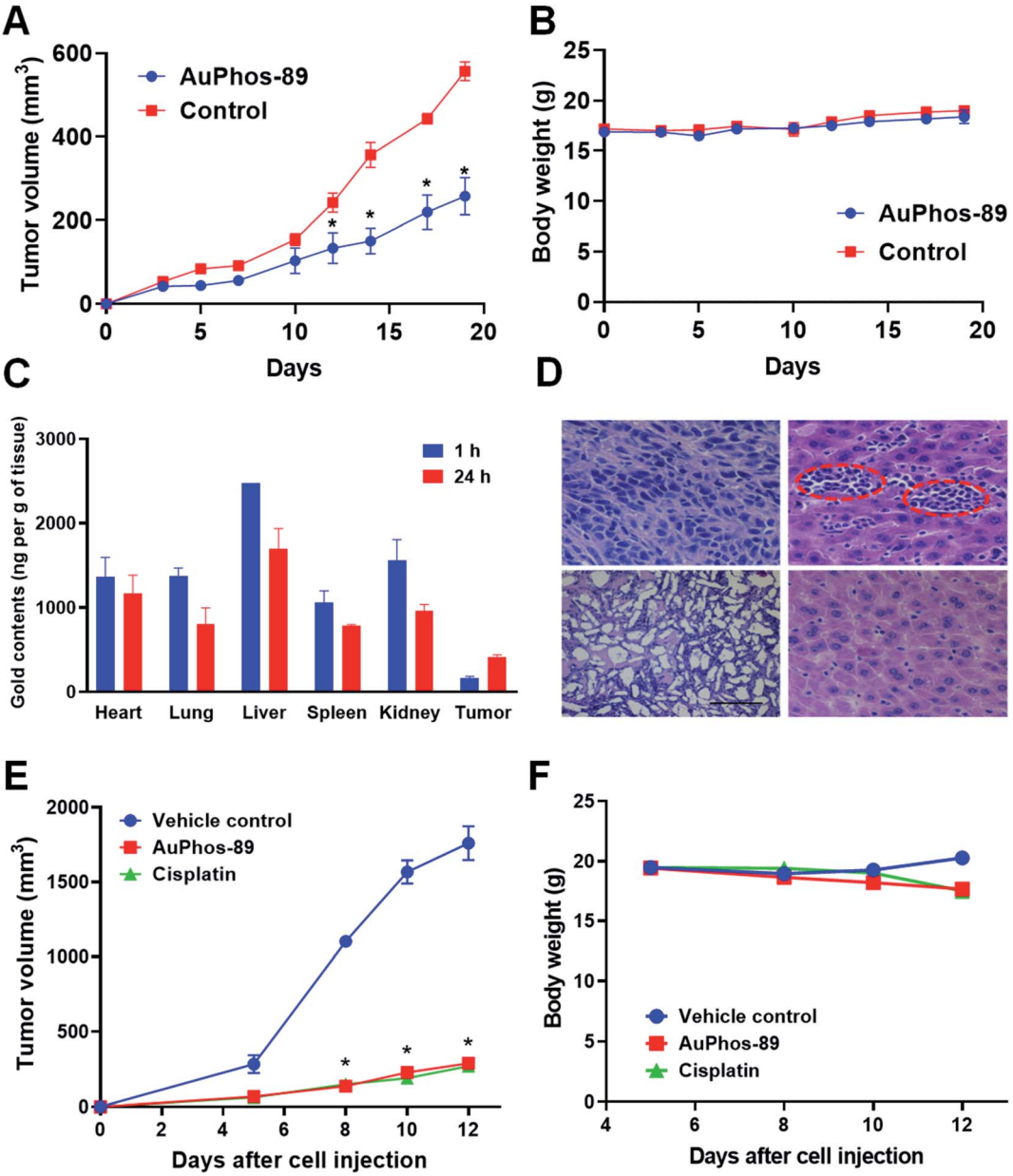

Fig. 7 Antitumor effect induced by **AuPhos-89**. (A) Impact of **AuPhos-89** on the tumor volume of 4T1 (1 million cells inoculated, $n = 5$). Unpaired t-test, $^*P < 0.05$. (B) Weight of mice ($n = 3$) following intravenous administration of **AuPhos-89** and observed over 19 days. (C) Tissue biodistribution of **AuPhos-89** in mice as determined by GF-AAS, which measures gold content. The compound was administered by intravenous injection and at indicated time points, tissues were collected after mice ($n = 3$) were euthanized. (D) Hematoxylin and eosin (H&E) staining indicates reduced cellularity and proliferation in tumors treated with **AuPhos-89**. Liver metastasis is observed in control mice with no palpable metastatic lesions in treated mice. (E) Comparative *in vivo* efficacy study of **AuPhos-89** and cisplatin. Impact of **AuPhos-89** and cisplatin on the tumor volume of 4T1 (two million cells inoculated, $n = 5$). Ordinary one-way ANOVA test, $^*P < 0.05$. (F) Weight of mice following intraperitoneal administration of **AuPhos-89** and cisplatin.

concentration was analyzed by GF-AAS. Furthermore, the relative quantification of Au levels (as measured by GF-AAS) in the different organs confirmed the uptake of **AuPhos-89** that had been introduced into separate mice *via* IV administration (Fig. 7B). These data give preliminary indication that **AuPhos-89** may travel in circulation to reach various organs. Further studies to determine metabolized or degraded gold compounds in circulation using detailed LC-MS/MS are underway.

Together, the data suggest that **AuPhos-89** induces significant tumor inhibition in 4T1 tumor bearing mice. Importantly, TNBC is an aggressive form of breast cancer with limited treatment options. Thus, therapeutic agents with different mechanisms of action could provide therapeutic benefit to patients. At the end of the observation period, mice in the **AuPhos-89** treatment arm did not exhibit significant change in their body weights, and histological tissue evaluation after H&E staining of excised tumor tissue shows high cellularity in the

treated group compared to vehicle control (Fig. 7D). Additionally, signs of liver metastasis were observed in control tissue, suggesting that **AuPhos-89** can inhibit liver metastasis associated with 4T1 tumors. Overall, AuPhos shows promise as a potent anticancer agent *in vivo*.

Conclusion

This report details the synthesis of novel gold(III)-bisphosphines that modulate mitochondrial respiration as anticancer agents *in vitro* and *in vivo*. Compounds that disrupt mitochondria with good pharmacokinetics and a wide therapeutic window remain an unmet need. Thus, a gold-based platform as a mitochondria respiration modulator holds promise as a useful therapeutic agent in a variety of diseases including cancer. The developed organometallic gold(III) compounds are relatively stable in solution even in the presence of physiologically relevant concentrations of glutathione, a major biological thiol. These complexes are potent across a wide range of cancer cell lines with significant lethality in the NCI-60 cell line with no cross-resistance. The compounds display high cellular uptake in cancer cells of >100 pmol per million cells. We used a systems biology approach to gain insight into the mechanism of action of the prioritized gold agent, **AuPhos-89**. The global effects of AuPhos on MDA-MB-231 cells identified biological processes related to oxidative phosphorylation, rheumatoid arthritis, Parkinsons disease, cytokine–cytokine receptor interaction, and NOD-like receptor signalling as prominent pathways by KEGG analysis. Using bioenergetics to assess mouse liver mitochondria and liver cancer cells, it was confirmed that AuPhos stimulates OCR leading to oxidative stress and, consequently, cell death *via* apoptosis. Therapeutic indices including the maximum tolerated dose, tissue biodistribution and efficacy reveal that AuPhos is a promising gold(III) anticancer agent.

Author contributions

S. O. performed the Western Blot and animal study. H. V. and J. H. K. accomplished mitochondria metabolism assay. H. V., P. G. S., J. H. K., and S. G. A. analyzed the mitochondria metabolism data. S. P. solved the X-ray structures of compounds. J. H. K. performed the synthesis and all characterization, stability assay and reactivity with GSH, cell viability assay, cellular/mitochondria uptake assay, differentially expressed gene/protein experiments, JC-1 assay, cell cycle, apoptosis, and animal experiments. J. H. K. and S. G. A. designed the project, analyzed the results, prepared figures, and wrote the manuscript.

Funding sources

We are grateful to the University of Kentucky for funding. The authors acknowledge the support of the Center for Pharmaceutical Research and Innovation (NIH P20 GM130456). The work was also supported by NIH R01NS112693-01A1 (PGS).

Conflicts of interest

The authors declare no competing financial interest.

Acknowledgements

Our study was performed in compliance with the NIH guidelines (NIH Publication No. 85-23 Rev. 1985) for the care and use of laboratory animals and all experimental procedures were monitored and approved by the Institutional Animal Care and Use Committee (IACUC) of the University of Kentucky (USA). We thank the UK NMR Center supported by NSF (CHE-997738) and the UK X-ray facility supported by the MRI program from NSF (CHE-1625732). For the flow cytometry analysis, we thank Dr Greg Bauman and the UK Flow Cytometry & Immune Monitoring core facility supported in part by the Office of the Vice President for Research, the Markey Cancer Center, and an NCI Center core support grant (P30 CA177558) to the University of Kentucky Markey Cancer Center. We thank Dr Tomoko Sengoku and Mr Michael Alstott for the redox metabolism analysis and their program supported by the Redox Metabolism Shared Resource Facility of the University of Kentucky Markey Cancer Center (P30 CA177558). We sincerely thank Dr Wendy Katz and Ms Megan A. Peterson for helping with H&E staining, and their research program supported by an Institutional Development Award (IDeA) from the National Institute of General Medical Sciences of the National Institutes of Health under grant number P30 GM127211. We also thank Dr Thomas Lee and the University of Colorado Boulder, College of Arts and Sciences, Mass Spectrometry Facility, for analyzing HRMS samples. We thank Dr Neeraj Kapur for providing the NCM460 cell. We also thank Ms Sailajah Gukathasan for helping with the LC-MS and Dr Steven Van Lanen of the UK College of Pharmacy, who allowed the use of the LC-MS.

References

1 B. Sirohi, S. Ashley, A. Norton, S. Popat, S. Hughes, P. Papadopoulos, K. Priest and M. O'Brien, Early Response to Platinum-Based First-Line Chemotherapy in Non-small Cell Lung Cancer May Predict Survival, *J. Thorac. Oncol.*, 2007, **2**(8), 735–740.

2 M. Li, Q. Zhang, P. Fu, P. Li, A. Peng, G. Zhang, X. Song, M. Tan, X. Li, Y. Liu, Y. Wu, S. Fan and C. Wang, Pemetrexed plus platinum as the first-line treatment option for advanced non-small cell lung cancer: a meta-analysis of randomized controlled trials, *PLoS One*, 2012, **7**(5), e37229.

3 V. Brabec and J. Kasparkova, Modifications of DNA by platinum complexes. Relation to resistance of tumors to platinum antitumor drugs. Drug resistance updates : reviews and commentaries in antimicrobial and anticancer chemotherapy, *Drug Resist. Updates*, 2005, **8**(3), 131–146.

4 Z. H. Siddik, Cisplatin: mode of cytotoxic action and molecular basis of resistance, *Oncogene*, 2003, **22**(47), 7265–7279.

5 S. R. McWhinney, R. M. Goldberg and H. L. McLeod, Platinum neurotoxicity pharmacogenetics, *Mol. Cancer Ther.*, 2009, **8**(1), 10–16.

6 I. Ott and R. Gust, Non platinum metal complexes as anti-cancer drugs, *Arch. Pharm.*, 2007, **340**(3), 117–126.
7 Y. Jung and S. J. Lippard, Direct cellular responses to platinum-induced DNA damage, *Chem. Rev.*, 2007, **107**(5), 1387–1407.
8 T. Zou, C. T. Lum, C.-N. Lok, J.-J. Zhang and C.-M. Che, Chemical biology of anticancer gold(III) and gold(I) complexes, *Chem. Soc. Rev.*, 2015, **44**(24), 8786–8801.
9 K.-C. Tong, C.-N. Lok, P.-K. Wan, D. Hu, Y. M. E. Fung, X.-Y. Chang, S. Huang, H. Jiang and C.-M. Che, An anticancer gold(III)-activated porphyrin scaffold that covalently modifies protein cysteine thiols, *Proc. Natl. Acad. Sci. U. S. A.*, 2020, **117**(3), 1321–1329.
10 J. Maksimoska, L. Feng, K. Harms, C. Yi, J. Kissil, R. Marmorstein and E. Meggers, Targeting large kinase active site with rigid, bulky octahedral ruthenium complexes, *J. Am. Chem. Soc.*, 2008, **130**(47), 15764–15765.
11 E. Meggers, Targeting proteins with metal complexes, *Chem. Commun.*, 2009, 1001–1010.
12 M. Dorr and E. Meggers, Metal complexes as structural templates for targeting proteins, *Curr. Opin. Chem. Biol.*, 2014, **19**, 76–81.
13 P. Zhang and P. J. Sadler, Redox-Active Metal Complexes for Anticancer Therapy, *Eur. J. Inorg. Chem.*, 2017, **2017**(12), 1541–1548.
14 N. Graf and S. J. Lippard, Redox activation of metal-based prodrugs as a strategy for drug delivery, *Adv. Drug Delivery Rev.*, 2012, **64**(11), 993–1004.
15 U. Jungwirth, C. R. Kowol, B. K. Keppler, C. G. Hartinger, W. Berger and P. Heffeter, Anticancer activity of metal complexes: involvement of redox processes, *Antioxid. Redox Signaling*, 2011, **15**(4), 1085–1127.
16 N. J. Farrer, L. Salassa and P. J. Sadler, Photoactivated chemotherapy (PACT): the potential of excited-state d-block metals in medicine, *Dalton Trans.*, 2009, 10690–10701.
17 K. D. Mjos and C. Orvig, Metallodrugs in Medicinal Inorganic Chemistry, *Chem. Rev.*, 2014, **114**(8), 4540–4563.
18 E. S. Antonarakis and A. Emadi, Ruthenium-based chemotherapeutics: are they ready for prime time?, *Cancer Chemother. Pharmacol.*, 2010, **66**(1), 1–9.
19 J. M. Rademaker-Lakhai, D. van den Bongard, D. Pluim, J. H. Beijnen and J. H. M. Schellens, A phase I and pharmacological study with imidazolium-trans-DMSO-imidazole-tetrachlororuthenate, a novel ruthenium anticancer agent, *Clin. Cancer Res.*, 2004, **10**(11), 3717–3727.
20 K. M. Knopf, B. L. Murphy, S. N. MacMillan, J. M. Baskin, M. P. Barr, E. Boros and J. J. Wilson, In vitro anticancer activity and *in vivo* biodistribution of rhenium(I) tricarbonyl aqua complexes, *J. Am. Chem. Soc.*, 2017, **139**(40), 14302–14314.
21 K. Suntharalingam, S. G. Awuah, P. M. Bruno, T. C. Johnstone, F. Wang, W. Lin, Y.-R. Zheng, J. E. Page, M. T. Hemann and S. J. Lippard, Necroptosis-Inducing Rhenium(V) Oxo Complexes, *J. Am. Chem. Soc.*, 2015, **137**(8), 2967–2974.
22 J. M. Hearn, I. Romero-Canelón, A. F. Munro, Y. Fu, A. M. Pizarro, M. J. Garnett, U. McDermott, N. O. Carragher and P. J. Sadler, Potent organo-osmium compound shifts metabolism in epithelial ovarian cancer cells, *Proc. Natl. Acad. Sci. U. S. A.*, 2015, **112**(29), E3800–E3805.
23 K. Suntharalingam, T. C. Johnstone, P. M. Bruno, W. Lin, M. T. Hemann and S. J. Lippard, Bidentate Ligands on Osmium(VI) Nitrido Complexes Control Intracellular Targeting and Cell Death Pathways, *J. Am. Chem. Soc.*, 2013, **135**(38), 14060–14063.
24 R. T. Mertens, S. Parkin and S. G. Awuah, Cancer cell-selective modulation of mitochondrial respiration and metabolism by potent organogold(III) dithiocarbamates, *Chem. Sci.*, 2020, **11**, 10465–10482.
25 S. Gukathasan, S. Parkin and S. G. Awuah, Cyclometalated Gold(III) Complexes Bearing DACH Ligands, *Inorg. Chem.*, 2019, **58**(14), 9326–9340.
26 J. H. Kim, E. Reeder, S. Parkin and S. G. Awuah, Gold(I/III)-Phosphine Complexes as Potent Antiproliferative Agents, *Sci. Rep.*, 2019, **9**(1), 12335.
27 I. Ott, On the medicinal chemistry of gold complexes as anticancer drugs, *Coord. Chem. Rev.*, 2009, **253**(11), 1670–1681.
28 I. Anvarhusein and P. J. Sadler, A carbon-13 nuclear magnetic resonance study of thiol-exchange reactions of gold(I) thiomalate ("Myocrisin") including applications to cysteine derivatives, *J. Chem. Soc., Dalton Trans.*, 1982, 135–141.
29 T. Zou, C. T. Lum, C. N. Lok, J. J. Zhang and C. M. Che, Chemical biology of anticancer gold(III) and gold(I) complexes, *Chem. Soc. Rev.*, 2015, **44**(24), 8786–8801.
30 S. Preiß, C. Förster, S. Otto, M. Bauer, P. Müller, D. Hinderberger, H. Hashemi Haeri, L. Carella and K. Heinze, Structure and reactivity of a mononuclear gold(II) complex, *Nat. Chem.*, 2017, **9**, 1249.
31 C.-Y. Wu, T. Horibe, C. B. Jacobsen and F. D. Toste, Stable gold(III) catalysts by oxidative addition of a carbon-carbon bond, *Nature*, 2015, **517**(7535), 449–454.
32 B. Bertrand, S. Spreckelmeyer, E. Bodio, F. Cocco, M. Picquet, P. Richard, P. Le Gendre, C. Orvig, M. A. Cinellu and A. Casini, Exploring the potential of gold(III) cyclometallated compounds as cytotoxic agents: variations on the C^N theme, *Dalton Trans.*, 2015, **44**(26), 11911–11918.
33 S. Carboni, A. Zucca, S. Stoccoro, L. Maiore, M. Arca, F. Ortu, C. Artner, B. K. Keppler, S. M. Meier-Menches, A. Casini and M. A. Cinellu, New Variations on the Theme of Gold(III) C(wedge)N(wedge)N Cyclometalated Complexes as Anticancer Agents: Synthesis and Biological Characterization, *Inorg. Chem.*, 2018, **57**(23), 14852–14865.
34 G. Marcon, S. Carotti, M. Coronnello, L. Messori, E. Mini, P. Orioli, T. Mazzei, M. A. Cinellu and G. Minghetti, Gold(III) complexes with bipyridyl ligands: solution chemistry, cytotoxicity, and DNA binding properties, *J. Med. Chem.*, 2002, **45**(8), 1672–1677.
35 L. Massai, D. Cirri, E. Michelucci, G. Bartoli, A. Guerri, M. A. Cinellu, F. Cocco, C. Gabbiani and L. Messori, Organogold(III) compounds as experimental anticancer

agents: chemical and biological profiles, *BioMetals*, 2016, **29**(5), 863–872.

36 L. Messori, G. Marcon, M. A. Cinellu, M. Coronnello, E. Mini, C. Gabbiani and P. Orioli, Solution chemistry and cytotoxic properties of novel organogold(III) compounds, *Bioorg. Med. Chem.*, 2004, **12**(23), 6039–6043.

37 R. T. Mertens, S. R. Parkin and S. G. Awuah, Synthesis and crystal structure of 1,3-bis-(4-hy-droxy-phen-yl)-1H-imidazole-3-ium chloride, *Acta Crystallogr., Sect. E: Crystallogr. Commun.*, 2019, **75**(Pt 9), 1311–1315.

38 J. H. Kim, R. T. Mertens, A. Agarwal, S. Parkin, G. Berger and S. G. Awuah, Direct intramolecular carbon(sp(2))-nitrogen(sp(2)) reductive elimination from gold(III), *Dalton Trans.*, 2019, **48**(18), 6273–6282.

39 R. T. Mertens, J. H. Kim, W. C. Jennings, S. Parkin and S. G. Awuah, Revisiting the reactivity of tetrachloroauric acid with N,N-bidentate ligands: structural and spectroscopic insights, *Dalton Trans.*, 2019, **48**(6), 2093–2099.

40 D. Hu, Y. Liu, Y.-T. Lai, K.-C. Tong, Y.-M. Fung, C.-N. Lok and C.-M. Che, Anticancer Gold(III) Porphyrins Target Mitochondrial Chaperone Hsp60, *Angew. Chem., Int. Ed.*, 2016, **55**(4), 1387–1391.

41 C.-M. Che, R. W.-Y. Sun, W.-Y. Yu, C.-B. Ko, N. Zhu and H. Sun, Gold(III) porphyrins as a new class of anticancer drugs: cytotoxicity, DNA binding and induction of apoptosis in human cervix epitheloid cancer cells, *Chem. Commun.*, 2003, 1718–1719.

42 A. D. Lammer, M. E. Cook and J. L. Sessler, Synthesis and anti-cancer activities of a water soluble gold(III) porphyrin, *J. Porphyrins Phthalocyanines*, 2015, **19**(1–3), 398–403.

43 K.-C. Tong, D. Hu, P.-K. Wan, C.-N. Lok and C.-M. Che, Anticancer Gold(III) Compounds with Porphyrin or N-heterocyclic Carbene Ligands, *Front. Chem.*, 2020, **8**(919), 587207.

44 I. Toubia, C. Nguyen, S. Diring, L. M. A. Ali, L. Larue, R. Aoun, C. Frochot, M. Gary-Bobo, M. Kobeissi and F. Odobel, Synthesis and Anticancer Activity of Gold Porphyrin Linked to Malonate Diamine Platinum Complexes, *Inorg. Chem.*, 2019, **58**(18), 12395–12406.

45 M. Serratrice, M. A. Cinellu, L. Maiore, M. Pilo, A. Zucca, C. Gabbiani, A. Guerri, I. Landini, S. Nobili, E. Mini and L. Messori, Synthesis, Structural Characterization, Solution Behavior, and *in Vitro* Antiproliferative Properties of a Series of Gold Complexes with 2-(2′-Pyridyl) benzimidazole as Ligand: Comparisons of Gold(III) *versus* Gold(I) and Mononuclear *versus* Binuclear Derivatives, *Inorg. Chem.*, 2012, **51**(5), 3161–3171.

46 J. R. Stenger-Smith and P. K. Mascharak, Gold Drugs with {Au(PPh_3)}+ Moiety: Advantages and Medicinal Applications, *ChemMedChem*, 2020, **15**(22), 2136–2145.

47 T. Srinivasa Reddy, S. H. Privér, V. V. Rao, N. Mirzadeh and S. K. Bhargava, Gold(I) and gold(III) phosphine complexes: synthesis, anticancer activities towards 2D and 3D cancer models, and apoptosis inducing properties, *Dalton Trans.*, 2018, **47**(43), 15312–15323.

48 M. A. Cinellu, A. Zucca, S. Stoccoro, G. Minghetti, M. Manassero and M. Sansoni, Synthesis and characterization of gold(III) adducts and cyclometallated derivatives with 2-substituted pyridines. Crystal structure of [Au{$NC_5H_4(CMe_2C_6H_4)$-2}Cl_2], *J. Chem. Soc., Dalton Trans.*, 1995, 2865–2872.

49 S. J. Berners-Price, C. K. Mirabelli, R. K. Johnson, M. R. Mattern, F. L. McCabe, L. F. Faucette, C. M. Sung, S. M. Mong, P. J. Sadler and S. T. Crooke, *In vivo* antitumor activity and *in vitro* cytotoxic properties of bis[1,2-bis(diphenylphosphino)ethane]gold(I) chloride, *Cancer Res.*, 1986, **46**(11), 5486–5493.

50 O. Rackham, S. J. Nichols, P. J. Leedman, S. J. Berners-Price and A. Filipovska, A gold(I) phosphine complex selectively induces apoptosis in breast cancer cells: implications for anticancer therapeutics targeted to mitochondria, *Biochem. Pharmacol.*, 2007, **74**(7), 992–1002.

51 S. J. Berners-Price, G. R. Girard, D. T. Hill, B. M. Sutton, P. S. Jarrett, L. F. Faucette, R. K. Johnson, C. K. Mirabelli and P. J. Sadler, Cytotoxicity and antitumor activity of some tetrahedral bis(diphosphino)gold(I) chelates, *J. Med. Chem.*, 1990, **33**(5), 1386–1392.

52 R. G. Buckley, A. M. Elsome, S. P. Fricker, G. R. Henderson, B. R. C. Theobald, R. V. Parish, B. P. Howe and L. R. Kelland, Antitumor Properties of Some 2-[(Dimethylamino)methyl] phenylgold(III) Complexes, *J. Med. Chem.*, 1996, **39**(26), 5208–5214.

53 H.-Q. Liu, T.-C. Cheung, S.-M. Peng and C.-M. Che, Novel luminescent cyclometaiated and terpyridine gold(III) complexes and DNA binding studies, *J. Chem. Soc., Chem. Commun.*, 1995, **17**, 1787–1788.

54 S. Carboni, A. Zucca, S. Stoccoro, L. Maiore, M. Arca, F. Ortu, C. Artner, B. K. Keppler, S. M. Meier-Menches, A. Casini and M. A. Cinellu, New Variations on the Theme of Gold(III) C^N^N Cyclometalated Complexes as Anticancer Agents: Synthesis and Biological Characterization, *Inorg. Chem.*, 2018, **57**(23), 14852–14865.

55 M. Frik, J. Fernández-Gallardo, O. Gonzalo, V. Mangas-Sanjuan, M. González-Alvarez, A. Serrano del Valle, C. Hu, I. González-Alvarez, M. Bermejo, I. Marzo and M. Contel, Cyclometalated Iminophosphorane Gold(III) and Platinum(II) Complexes. A Highly Permeable Cationic Platinum(II) Compound with Promising Anticancer Properties, *J. Med. Chem.*, 2015, **58**(15), 5825–5841.

56 S. K. Fung, T. Zou, B. Cao, P. Y. Lee, Y. M. Fung, D. Hu, C. N. Lok and C. M. Che, Cyclometalated Gold(III) Complexes Containing N-Heterocyclic Carbene Ligands Engage Multiple Anti-Cancer Molecular Targets, *Angew. Chem.*, 2017, **56**(14), 3892–3896.

57 L. Massai, D. Cirri, E. Michelucci, G. Bartoli, A. Guerri, M. A. Cinellu, F. Cocco, C. Gabbiani and L. Messori, Organogold(III) compounds as experimental anticancer agents: chemical and biological profiles, *BioMetals*, 2016, **29**(5), 863–872.

58 R. Kumar and C. Nevado, Cyclometalated Gold(III) Complexes: Synthesis, Reactivity, and Physicochemical Properties, *Angew. Chem., Int. Ed.*, 2017, **56**(8), 1994–2015.

59 S. Gukathasan, S. Parkin and S. G. Awuah, Cyclometalated Gold(III) Complexes Bearing DACH Ligands, *Inorg. Chem.*, 2019, **58**(14), 9326–9340.

60 E. K. Dennis, J. H. Kim, S. Parkin, S. G. Awuah and S. Garneau-Tsodikova, Distorted Gold(I)-Phosphine Complexes as Antifungal Agents, *J. Med. Chem.*, 2020, **63**(5), 2455–2469.

61 D. Jia, M. Lu, K. H. Jung, J. H. Park, L. Yu, J. N. Onuchic, B. A. Kaipparettu and H. Levine, Elucidating cancer metabolic plasticity by coupling gene regulation with metabolic pathways, *Proc. Natl. Acad. Sci. U. S. A.*, 2019, **116**(9), 3909–3918.

62 J. H. Park, S. Vithayathil, S. Kumar, P.-L. Sung, L. E. Dobrolecki, V. Putluri, V. B. Bhat, S. K. Bhowmik, V. Gupta, K. Arora, D. Wu, E. Tsouko, Y. Zhang, S. Maity, T. R. Donti, B. H. Graham, D. E. Frigo, C. Coarfa, P. Yotnda, N. Putluri, A. Sreekumar, M. T. Lewis, C. J. Creighton, L.-J. C. Wong and B. A. Kaipparettu, Fatty Acid Oxidation-Driven Src Links Mitochondrial Energy Reprogramming and Oncogenic Properties in Triple-Negative Breast Cancer, *Cell Rep.*, 2016, **14**(9), 2154–2165.

63 V. S. LeBleu, J. T. O'Connell, K. N. Gonzalez Herrera, H. Wikman, K. Pantel, M. C. Haigis, F. M. de Carvalho, A. Damascena, L. T. Domingos Chinen, R. M. Rocha, J. M. Asara and R. Kalluri, PGC-1α mediates mitochondrial biogenesis and oxidative phosphorylation in cancer cells to promote metastasis, *Nat. Cell Biol.*, 2014, **16**(10), 992–1003.

64 P. E. Porporato, V. L. Payen, J. Pérez-Escuredo, C. J. De Saedeleer, P. Danhier, T. Copetti, S. Dhup, M. Tardy, T. Vazeille, C. Bouzin, O. Feron, C. Michiels, B. Gallez and P. Sonveaux, A Mitochondrial Switch Promotes Tumor Metastasis, *Cell Rep.*, 2014, **8**(3), 754–766.

65 R. Camarda, A. Y. Zhou, R. A. Kohnz, S. Balakrishnan, C. Mahieu, B. Anderton, H. Eyob, S. Kajimura, A. Tward, G. Krings, D. K. Nomura and A. Goga, Inhibition of fatty acid oxidation as a therapy for MYC-overexpressing triple-negative breast cancer, *Nat. Med.*, 2016, **22**(4), 427–432.

66 S. E. Weinberg and N. S. Chandel, Targeting mitochondria metabolism for cancer therapy, *Nat. Chem. Biol.*, 2015, **11**(1), 9–15.

67 J. Lee, A. E. Yesilkanal, J. P. Wynne, C. Frankenberger, J. Liu, J. Yan, M. Elbaz, D. C. Rabe, F. D. Rustandy, P. Tiwari, E. A. Grossman, P. C. Hart, C. Kang, S. M. Sanderson, J. Andrade, D. K. Nomura, M. G. Bonini, J. W. Locasale and M. R. Rosner, Effective breast cancer combination therapy targeting BACH1 and mitochondrial metabolism, *Nature*, 2019, **568**(7751), 254–258.

68 G. Libby, L. A. Donnelly, P. T. Donnan, D. R. Alessi, A. D. Morris and J. M. M. Evans, New users of metformin are at low risk of incident cancer. A cohort study among people with type 2 diabetes, *Diabetes Care*, 2009, **32**(9), 1620–1625.

69 W. W. Wheaton, S. E. Weinberg, R. B. Hamanaka, S. Soberanes, L. B. Sullivan, E. Anso, A. Glasauer, E. Dufour, G. M. Mutlu, G. R. S. Budigner and N. S. Chandel, Metformin inhibits mitochondrial complex I of cancer cells to reduce tumorigenesis, *eLife*, 2014, **3**, e02242.

70 A. Naguib, G. Mathew, C. R. Reczek, K. Watrud, A. Ambrico, T. Herzka, I. C. Salas, M. F. Lee, N. El-Amine, W. Zheng, M. E. Di Francesco, J. R. Marszalek, D. J. Pappin, N. S. Chandel and L. C. Trotman, Mitochondrial Complex I Inhibitors Expose a Vulnerability for Selective Killing of Pten-Null Cells, *Cell Rep.*, 2018, **23**(1), 58–67.

71 J. R. Molina, Y. Sun, M. Protopopova, S. Gera, M. Bandi, C. Bristow, T. McAfoos, P. Morlacchi, J. Ackroyd, A.-N. A. Agip, G. Al-Atrash, J. Asara, J. Bardenhagen, C. C. Carrillo, C. Carroll, E. Chang, S. Ciurea, J. B. Cross, B. Czako, A. Deem, N. Daver, J. F. de Groot, J.-W. Dong, N. Feng, G. Gao, J. Gay, M. G. Do, J. Greer, V. Giuliani, J. Han, L. Han, V. K. Henry, J. Hirst, S. Huang, Y. Jiang, Z. Kang, T. Khor, S. Konoplev, Y.-H. Lin, G. Liu, A. Lodi, T. Lofton, H. Ma, M. Mahendra, P. Matre, R. Mullinax, M. Peoples, A. Petrocchi, J. Rodriguez-Canale, R. Serreli, T. Shi, M. Smith, Y. Tabe, J. Theroff, S. Tiziani, Q. Xu, Q. Zhang, F. Muller, R. A. DePinho, C. Toniatti, G. F. Draetta, T. P. Heffernan, M. Konopleva, P. Jones, M. E. Di Francesco and J. R. Marszalek, An inhibitor of oxidative phosphorylation exploits cancer vulnerability, *Nat. Med.*, 2018, **24**(7), 1036–1046.

72 X. Liu, I. L. Romero, L. M. Litchfield, E. Lengyel and J. W. Locasale, Metformin Targets Central Carbon Metabolism and Reveals Mitochondrial Requirements in Human Cancers, *Cell Metab.*, 2016, **24**(5), 728–739.

73 S. R. Lord, W.-C. Cheng, D. Liu, E. Gaude, S. Haider, T. Metcalf, N. Patel, E. J. Teoh, F. Gleeson, K. Bradley, S. Wigfield, C. Zois, D. R. McGowan, M.-L. Ah-See, A. M. Thompson, A. Sharma, L. Bidaut, M. Pollak, P. G. Roy, F. Karpe, T. James, R. English, R. F. Adams, L. Campo, L. Ayers, C. Snell, I. Roxanis, C. Frezza, J. D. Fenwick, F. M. Buffa and A. L. Harris, Integrated Pharmacodynamic Analysis Identifies Two Metabolic Adaption Pathways to Metformin in Breast Cancer, *Cell Metab.*, 2018, **28**(5), 679–688.

74 Y. Shi, S. K. Lim, Q. Liang, S. V. Iyer, H. Y. Wang, Z. Wang, X. Xie, D. Sun, Y. J. Chen, V. Tabar, P. Gutin, N. Williams, J. K. De Brabander and L. F. Parada, Gboxin is an oxidative phosphorylation inhibitor that targets glioblastoma, *Nature*, 2019, **567**(7748), 341–346.

75 K. D. Paull, R. H. Shoemaker, L. Hodes, A. Monks, D. A. Scudiero, L. Rubinstein, J. Plowman and M. R. Boyd, Display and analysis of patterns of differential activity of drugs against human tumor cell lines: development of mean graph and COMPARE algorithm, *J. Natl. Cancer Inst.*, 1989, **81**(14), 1088–1092.

76 R. H. Shoemaker, The NCI60 human tumour cell line anticancer drug screen, *Nat. Rev. Cancer*, 2006, **6**(10), 813–823.

77 M. Kanehisa and S. Goto, KEGG: Kyoto Encyclopedia of Genes and Genomes, *Nucleic Acids Res.*, 2000, **28**(1), 27–30.

78 M. Kanehisa, Toward understanding the origin and evolution of cellular organisms, *Protein Sci.*, 2019, **28**(11), 1947–1951.

79 M. Kanehisa, Y. Sato, M. Furumichi, K. Morishima and M. Tanabe, New approach for understanding genome variations in KEGG, *Nucleic Acids Res.*, 2018, **47**(D1), D590–D595.